Supporting Information

Wearable System Integrating Dual Piezoresistive and Photoplethysmography Sensors for Simultaneous Pulse Wave Monitoring

Borzooye Jafarizadeh [1], Azmal Huda Chowdhury [1], Md Shariful Islam Sozal [1], Zhe Cheng [1], Nezih Pala [2], and Chunlei Wang [1, 3*]

[1] Department of Mechanical and Materials Engineering, Florida International University, Miami, FL 33174, USA

[2] Department of Electrical and Computer Engineering, Florida International University, Miami, FL 33174, USA

[3] Department of Mechanical and Aerospace Engineering, University of Miami, Coral Gables, FL 33146, USA

* Correspondence: wangc@miami.edu

Simulation method:

COMSOL evaluates and numerically solves the controlling partial differential equations using FEA. Generally, in the modelling, the governing partial differential equations are formulated either in a spatial coordinate system (Eulerian formulation), or material coordinate system (Lagrangian formulation) following the materials as it deforms. Herein, due to the extent of the deformation, the mapping from mesh (the process of turning irregular shapes into more recognizable volumes) coordinates to spatial coordinates could get ill-conditioned as the deformation progresses (a drawback of Lagrangian method). To alleviate this, a method called Arbitrary Lagrangian-Eulerian (ALE) is utilized. To ensure that the mapping of the quantities is always associated with a regular-shaped mesh, this method stops the simulation, deletes the previous mesh, and generates a new one. ALE is a dynamic middle approach that combines the best aspects of both Eulerian and Lagrangian methods depending on the needs of the inquiry. To investigate the effect of different base resistance (resistance at a preset 100 Pa applied pressure) of sensing materials on the signal output, a steady state modeling method was proposed. This modelling is designed to simulate the pulse wave pressure regimes experienced while the sensor is mounted on the wrist[1].

Details regarding the pulse waveform expressed in terms of resistance change (by the sourcemeter and wearable sensing system):

For the sourcemeter, the conversion was done using Ohm's law (V = IR) with measurements taken via the 4-wire method. This ensures highly accurate resistance readings by eliminating the influence of lead resistance. In contrast, for the wearable sensing system, the resistance change was calculated using the voltage divider formula, as the system operates with a 50-ohm voltage divider circuit:

$$R_{sensor} = R_{ref} \times \left(\frac{V_{in} - V_{supply}}{V_{in}}\right)$$

where, R_{ref} is 50 Ω, V_{in} is the voltage that is measured between the resistors in the voltage divider and V_{supply} is 3.3 V in this circuit.

Due to the differences in measurement methodology between the two systems, we observe some variation in the resistance change range between the sourcemeter and the wearable sensing system. However, given that the wearable sensing system successfully detects all the distinct peaks of the pulse waveform (systolic, diastolic notch, and diastolic peak) similar to the sourcemeter, it is appropriate to claim that the wearable system enjoys comparable resolution in capturing the details of the pulse waveform.

Figure S1

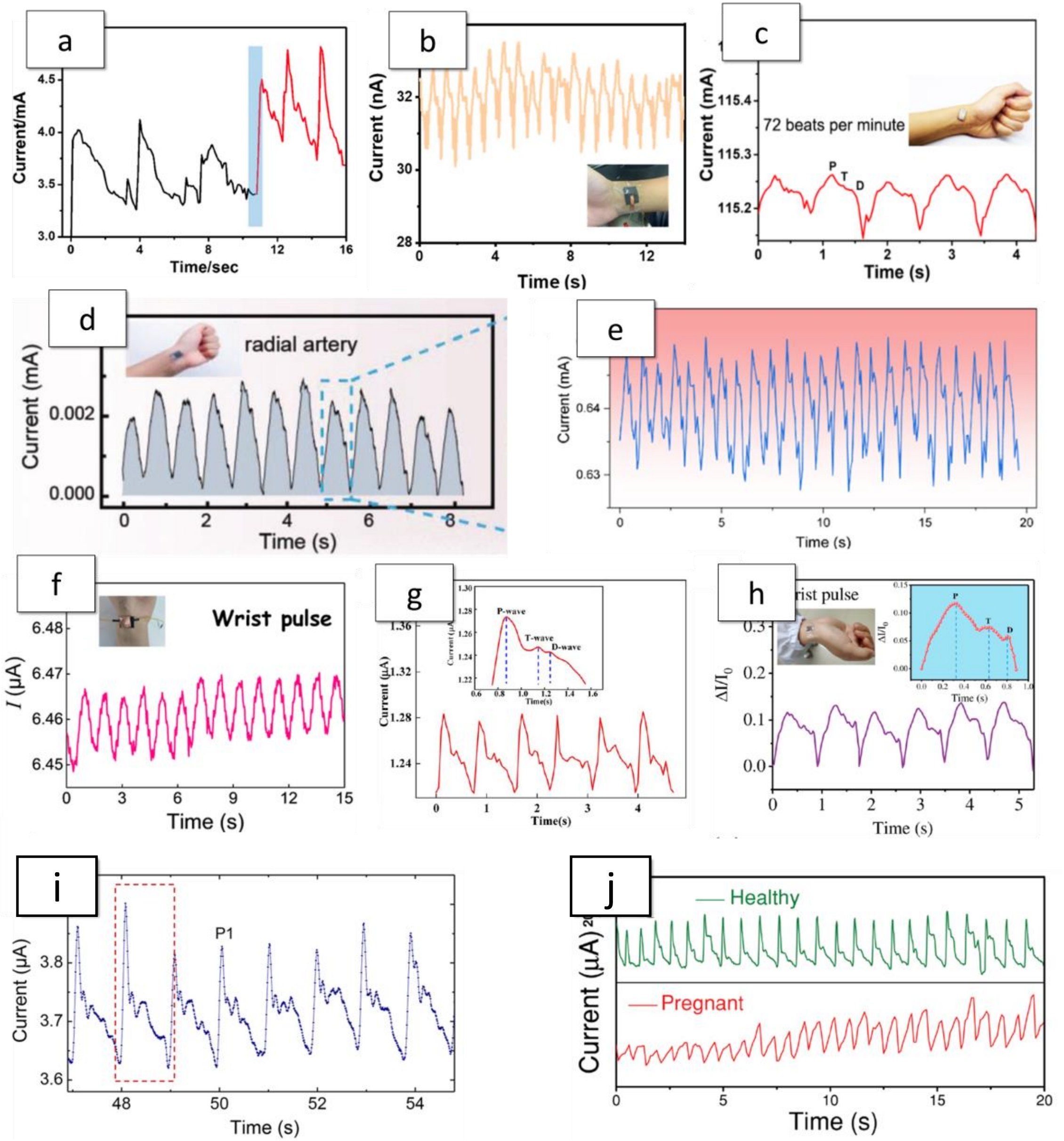

Figure S1. Plots of wrist pulse waveform acquired by piezoresistive sensors in the literature (a-j) [2-11].

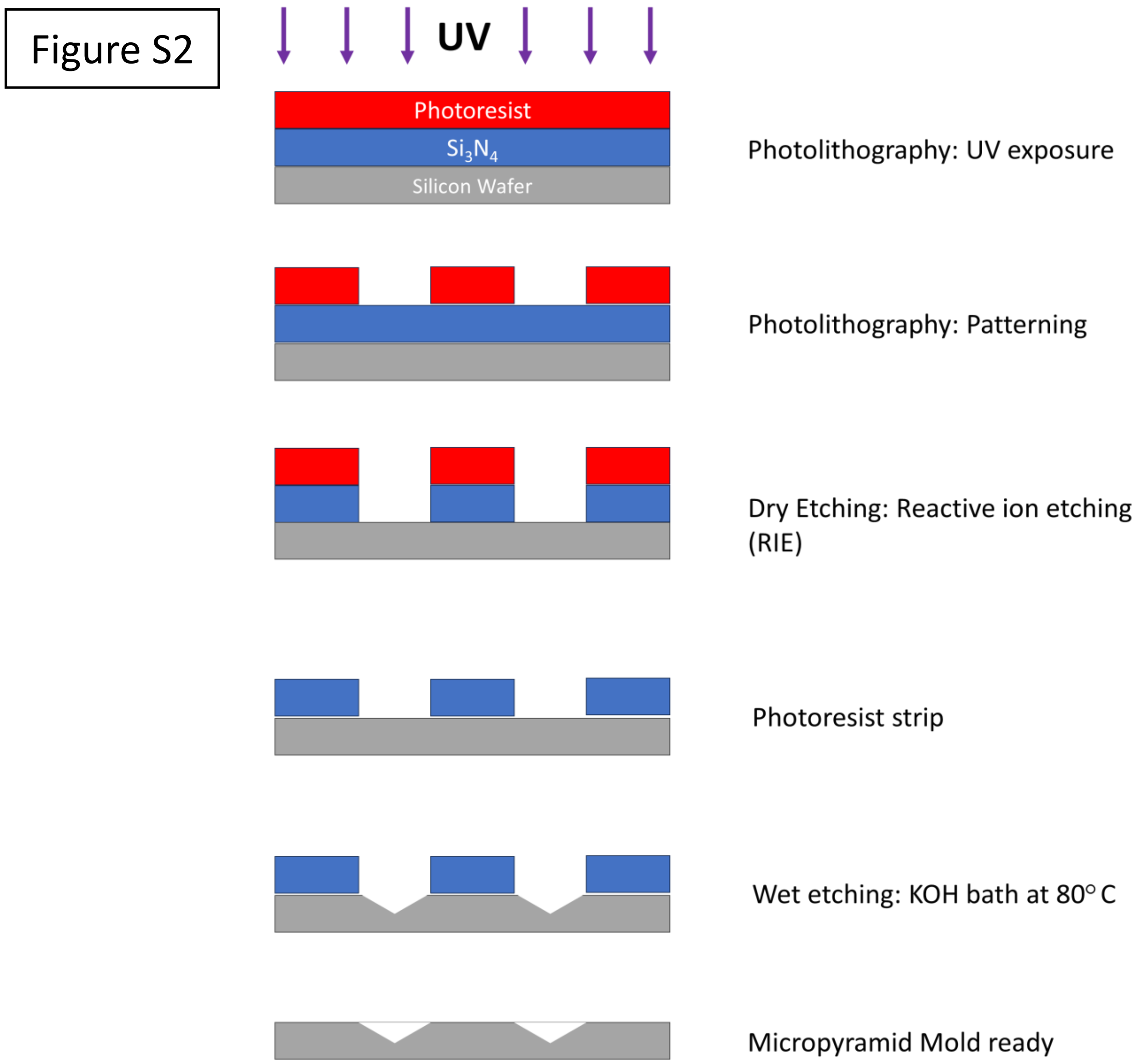

Figure S2. Operational steps to fabricate the micro-pyramid mold in silicon wafer.

Figure S3

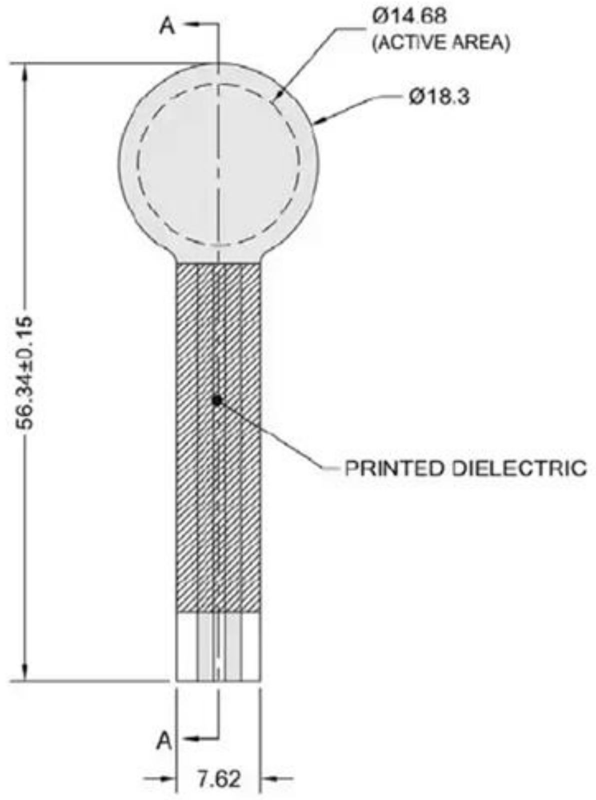

Figure S3. Interdigitated Electrode dimensions [12].

Figure S4

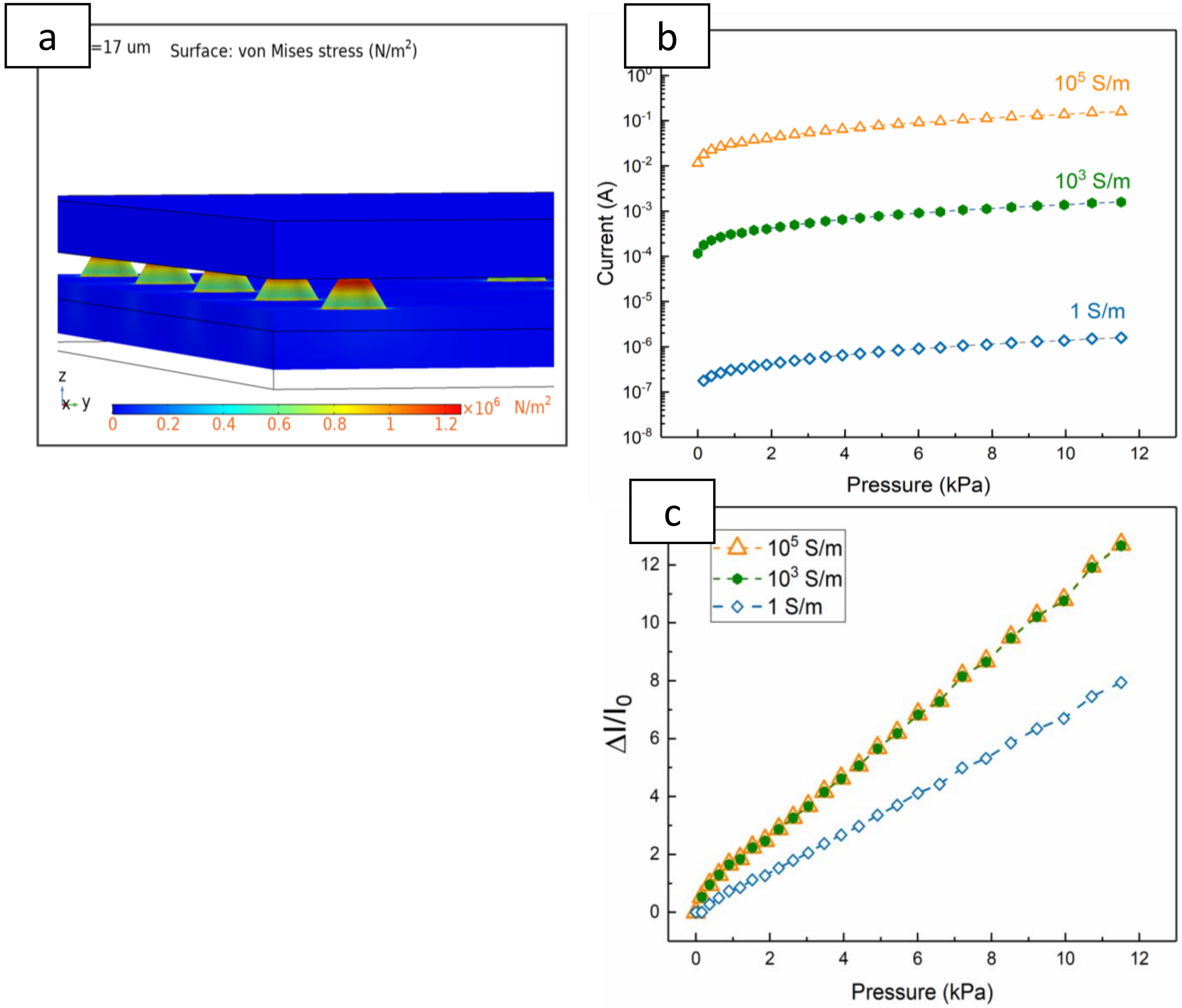

Figure S4: Pressure response analysis of micro-featured piezoresistive sensors with varying conductivity values. Includes 3D model (a), current response (b), and normalized current change (c) under compression.

Figure S5

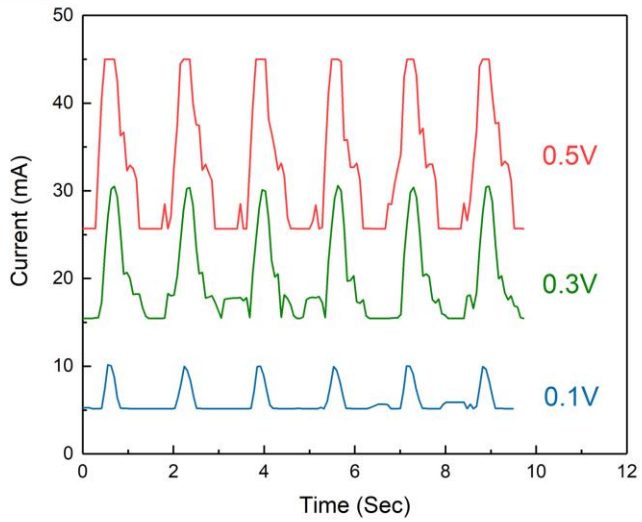

Figure S5. Dependency of signal detection capability at constant sampling rates on supplied voltage, using a consistent mechanical excitation signal.

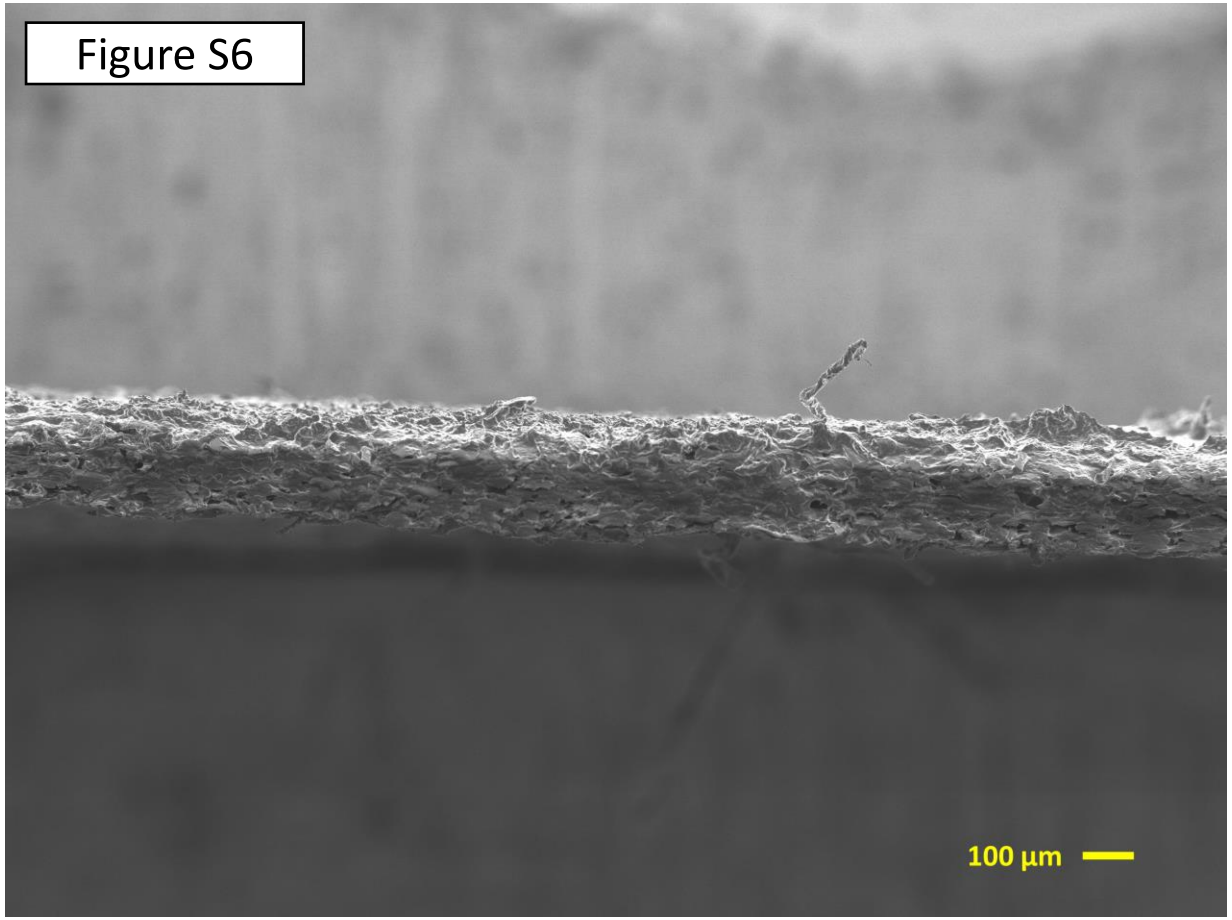

Figure S6. The SEM view of the cross section of the porous piezoresistive component of the dual piezoresistive sensor.

Figure S7

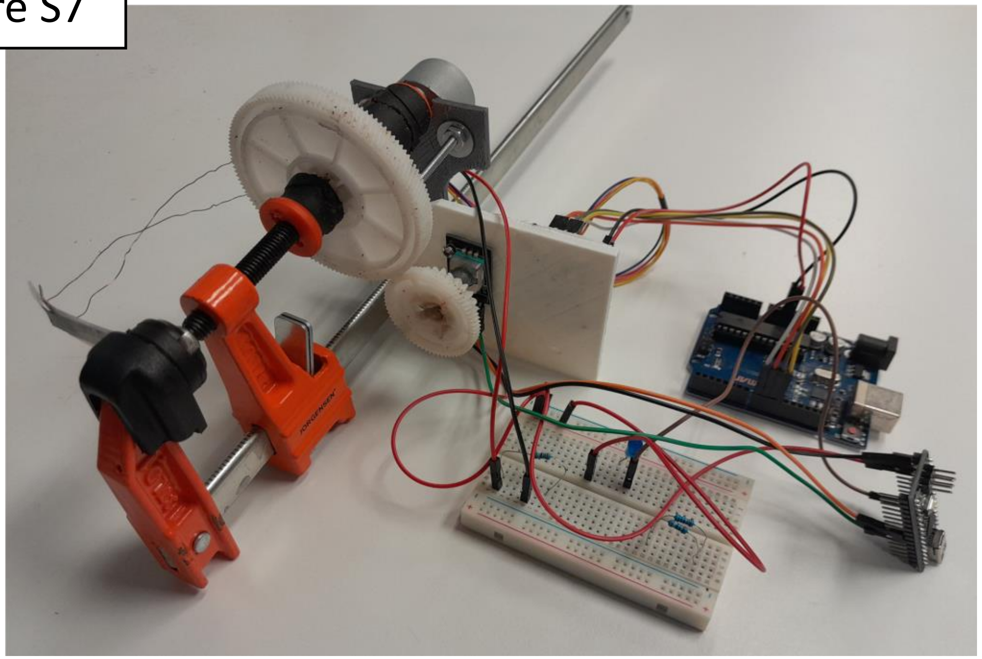

Figure S7. The mechanical testbed used for response time and cyclability measurement.

Figure S8

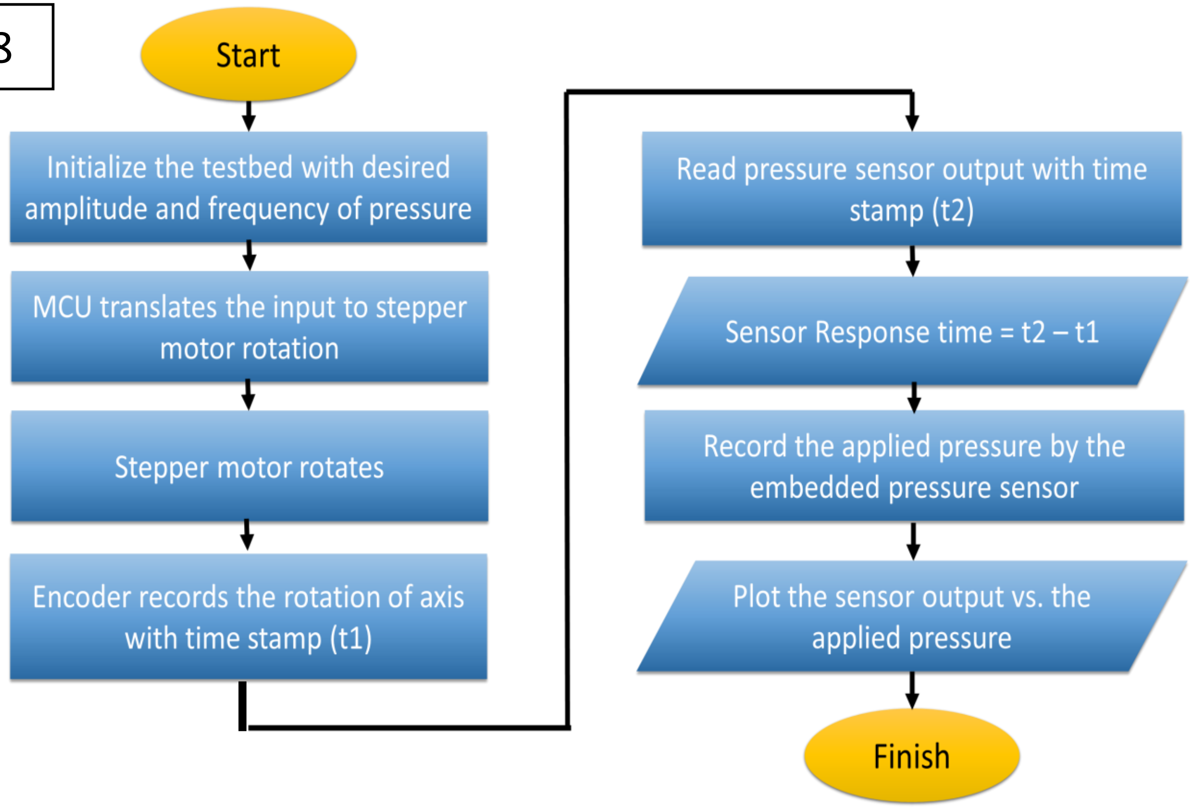

Figure S8. Flowchart illustrating the operational steps of the mechanical testbed used to measure response time.

Figure S9

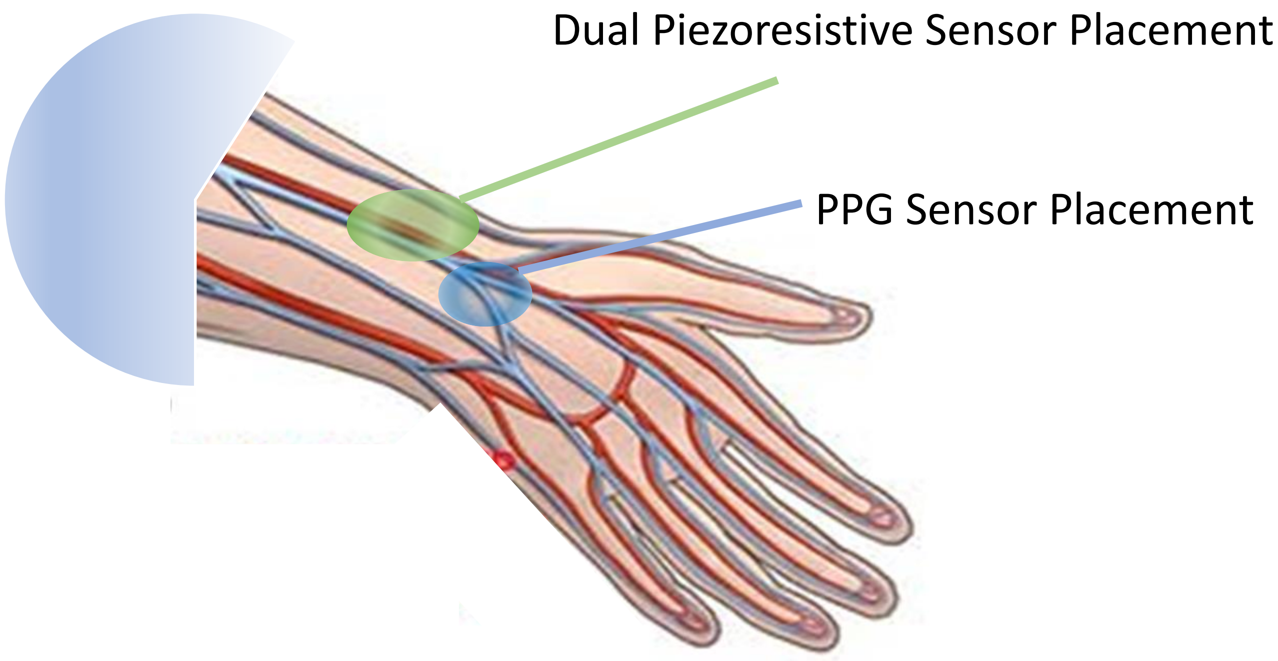

Figure S9. The placement of PPG (on top of cephalic vein) and dual piezoresistive senor (on top of radial artery) for capturing forward going and backward going blood flow.

Figure S10

Figure S10. Methodology for fabrication of porous conductive component of the dual piezoresistive pressure sensor.

Figure S11

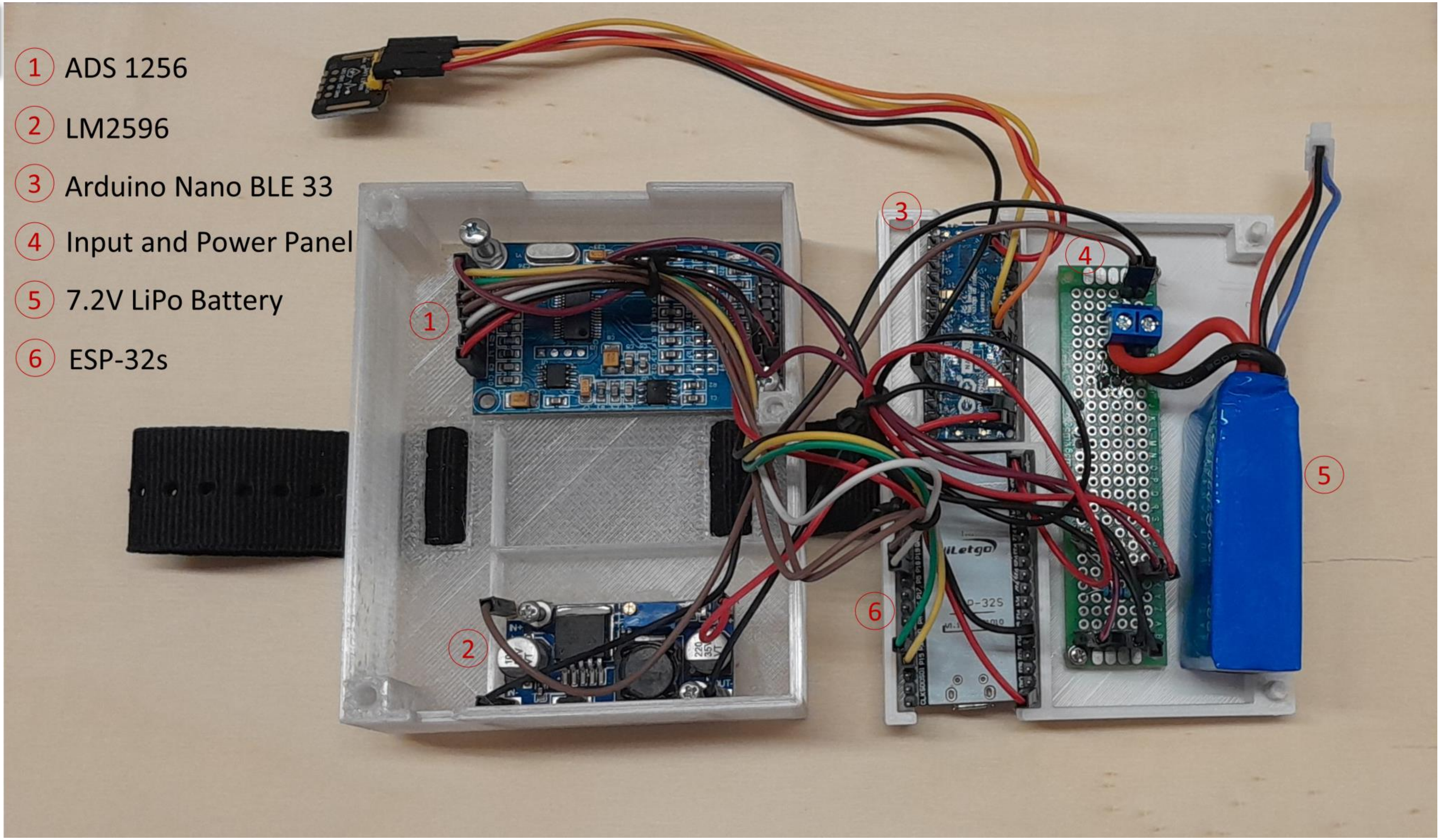

Figure S11. Internal components of the wearable sensing system.

Video S1

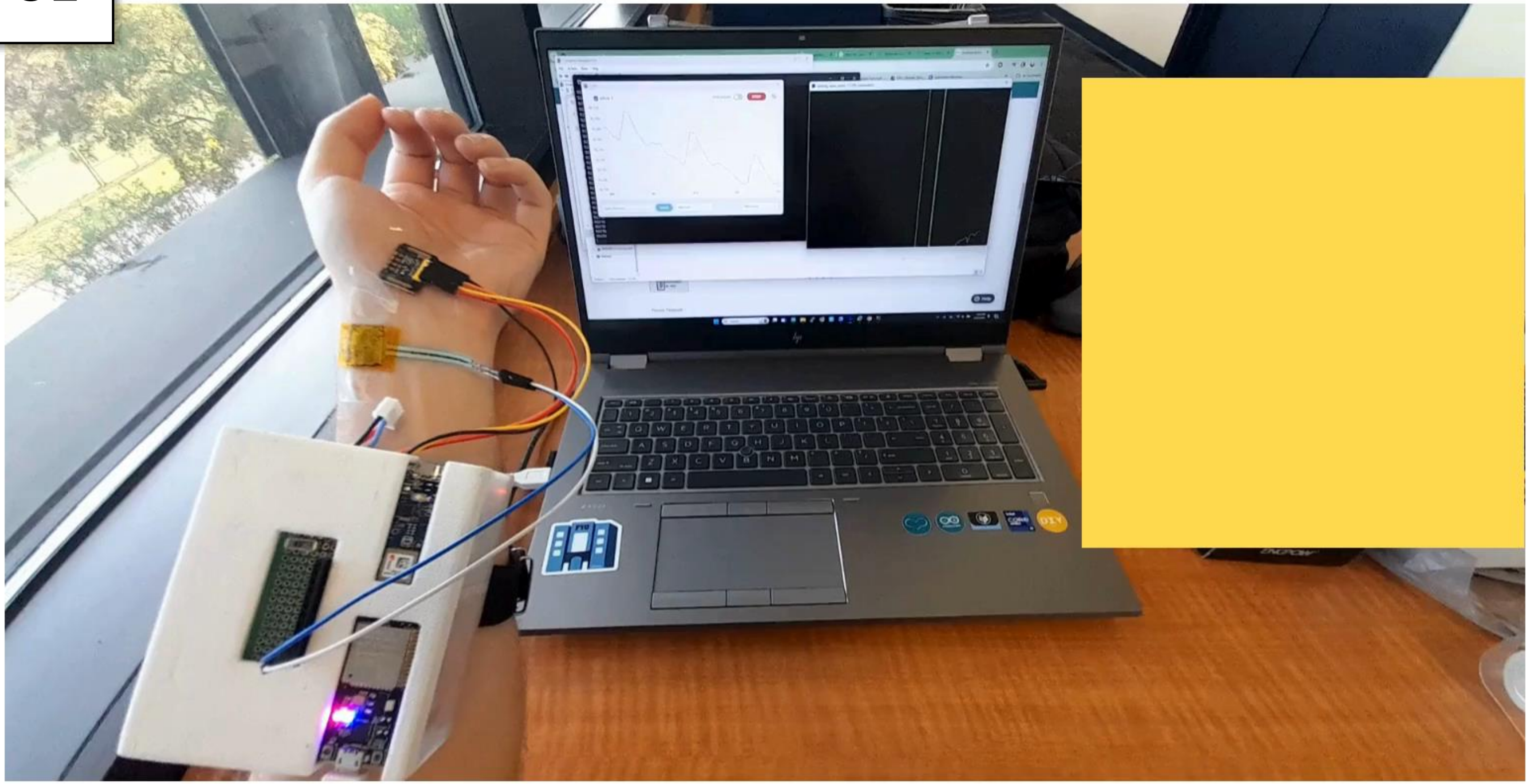

Video S1. Simultaneous pulse waveform detection by PPG and dual piezoresistive sensors on the same artery.

Video S2

Video S2. Dual piezoresistive sensor on the ankle, capturing pulse waveform and transmitting data to the computer in real time.

Video S3

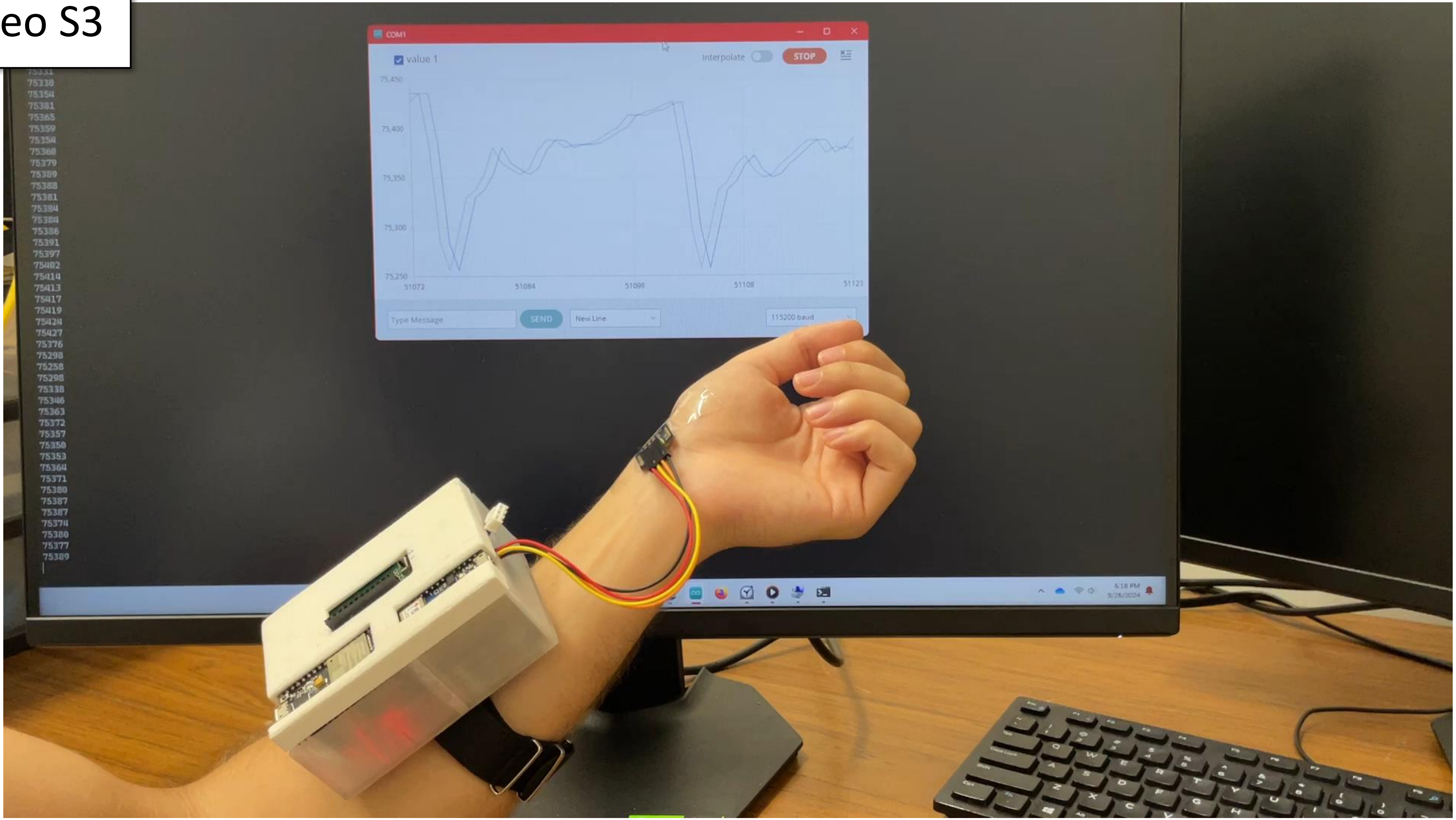

Video S3. Video demonstrating the induced noise caused by the proximity of IR radiation. The device, an MH-Sensor-Series IR obstacle detector, generates pulsating (5 Hz) IR radiation.

Table S1. Table summarizing the state of the art of piezoresistive pressure sensors with comparable structure to this study

TableS1

Piezoresistive Type	*Material/Feature*	*Sensitivity (kPa^{-1})*	*Stability (cycles)*	*Year/Ref.*
Porous	Graphene/Polyurethane Sponge	3.08	>10 000	[13]
Porous	Silver Nanowire Paper-based	1.5	NR	[14]
Porous	Biocarbon and Nylon	0.02	8000	[15]
Porous	Polypyrrole/Silver Nanowire Aero-Sponge	0.33	50	[16]
Micro-feature	From Plant Mold (Konjac leaf)	0.43	NR	[17]
Micro-feature	From Plant Mold (Banana leaf)	3.3	10 000	[18]
Micro-feature	From Plant Mold (Pollen)	3.5	9000	[19]
Micro-feature	From Photolithography Mold (Pyramid)	13.8	400	[20]
Micro-feature	From Photolithography Mold (Pyramid)	4.2	2000	[21]
Micro-feature	From 3D printing Mold (Semi-cylinder)	3.6	10 000	[22]
Micro-feature	From Laser Mold (Micro-ridge)	1.82	6000	[23]
Micro-feature	From Silk Mold	1.8	>67 500	[24]
Micro-feature	From Plant Mold (Papillae)	1.2	>1000	[25]
Dual Piezoresistive Pressure Sensor	Carbon black grease on Filter paper + From Photolithography Mold (Pyramid)	8.4	5000	[This work]

References

1. Multiphysics, C.M.-C.; Burlington, undefined; MA, undefined; accessed, undefined; 1998, undefined Introduction to Comsol Multiphysics®. academia.edu.
2. Yu, Z.; Xu, J.; Gong, H.; Li, Y.; Li, L.; Wei, Q.; Tang, D. Bioinspired Self-Powered Piezoresistive Sensors for Simultaneous Monitoring of Human Health and Outdoor UV Light Intensity. ACS Appl Mater Interfaces 2022, 14, 5101–5111, doi:10.1021/ACSAMI.1C23604/ASSET/IMAGES/LARGE/AM1C23604_0009.JPEG.
3. Yang, G.; Yang, Y.; Chen, T.; Wang, J.; Ma, L.; Yang, S. Graphene/MXene Composite Aerogels Reinforced by Polyimide for Pressure Sensing. ACS Appl Nano Mater 2022, 5, 1068–1077, doi:10.1021/ACSANM.1C03722/ASSET/IMAGES/LARGE/AN1C03722_0007.JPEG.
4. Sun, Q.J.; Zhao, X.H.; Yeung, C.C.; Tian, Q.; Kong, K.W.; Wu, W.; Venkatesh, S.; Li, W.J.; Roy, V.A.L. Bioinspired, Self-Powered, and Highly Sensitive Electronic Skin for Sensing Static and Dynamic Pressures. ACS Appl Mater Interfaces 2020, 12, 37239–37247, doi:10.1021/ACSAMI.0C10788/ASSET/IMAGES/LARGE/AM0C10788_0006.JPEG.
5. Li, L.; Bao, X.; Meng, J.; Zhang, C.; Liu, T. Sponge-Hosting Polyaniline Array Microstructures for Piezoresistive Sensors with a Wide Detection Range and High Sensitivity. ACS Appl Mater Interfaces 2022, 14, 30228–30235, doi:10.1021/ACSAMI.2C07404/ASSET/IMAGES/LARGE/AM2C07404_0006.JPEG.
6. Liu, Y.; Xu, H.; Dong, M.; Han, R.; Tao, J.; Bao, R.; Pan, C. Highly Sensitive Wearable Pressure Sensor Over a Wide Sensing Range Enabled by the Skin Surface-Like 3D Patterned Interwoven Structure. Adv Mater Technol 2022, 7, 2200504, doi:10.1002/ADMT.202200504.
7. Huang, J.; Zeng, J.; Liang, B.; Wu, J.; Li, T.; Li, Q.; Feng, F.; Feng, Q.; Rood, M.J.; Yan, Z. Multi-Arch-Structured All-Carbon Aerogels with Superelasticity and High Fatigue Resistance as Wearable Sensors. ACS Appl Mater Interfaces 2020, 12, 16822–16830, doi:10.1021/ACSAMI.0C01794/ASSET/IMAGES/LARGE/AM0C01794_0006.JPEG.
8. Choong, C.; Shim, M.; Lee, B.; … S.J.-A.; 2014, undefined Highly Stretchable Resistive Pressure Sensors Using a Conductive Elastomeric Composite on a Micropyramid Array. Wiley Online Library 2014, 26, 3451–3458, doi:10.1002/adma.201305182.
9. Wang, X.; Gu, Y.; Xiong, Z.; Cui, Z.; Zhang, T. Silk-Molded Flexible, Ultrasensitive, and Highly Stable Electronic Skin for Monitoring Human Physiological Signals. Advanced Materials 2014, 26, 1336–1342, doi:10.1002/ADMA.201304248.
10. Chang, H.; Kim, S.; Jin, S.; Lee, S.W.; Yang, G.T.; Lee, K.Y.; Yi, H. Ultrasensitive and Highly Stable Resistive Pressure Sensors with Biomaterial-Incorporated Interfacial Layers for Wearable Health-Monitoring and Human-Machine Interfaces. ACS Appl Mater Interfaces 2018, 10, 1067–1076, doi:10.1021/acsami.7b14048.
11. Park, J.; Kim, M.; Lee, Y.; Lee, H.; advances, H.K.-S.; 2015, undefined Fingertip Skin–Inspired Microstructured Ferroelectric Skins Discriminate Static/Dynamic Pressure and Temperature Stimuli. advances.sciencemag.org, doi:10.1126/sciadv.1500661.
12. FSR® 400 Series by Interlink Electronics Datasheet | DigiKey Available online: https://www.digikey.com/en/htmldatasheets/production/1184367/0/0/1/34-00022 (accessed on 16 June 2024).

13. Luo, Y.; Xiao, Q.; Li, B. Highly Compressible Graphene/Polyurethane Sponge with Linear and Dynamic Piezoresistive Behavior. RSC Adv 2017, 7, 34939–34944, doi:10.1039/C7RA03922K.
14. Gao, L.; Zhu, C.; Li, L.; Zhang, C.; Liu, J.; Yu, H.D.; Huang, W. All Paper-Based Flexible and Wearable Piezoresistive Pressure Sensor. ACS Appl Mater Interfaces 2019, 11, 25034–25042, doi:10.1021/ACSAMI.9B07465/SUPPL_FILE/AM9B07465_SI_001.PDF.
15. Tolvanen, J.; Kilpijärvi, J.; Pitkänen, O.; Hannu, J.; Jantunen, H. Stretchable Sensors with Tunability and Single Stimuli-Responsiveness through Resistivity Switching under Compressive Stress. ACS Appl Mater Interfaces 2020, 12, 14433–14442, doi:10.1021/ACSAMI.0C00023/ASSET/IMAGES/LARGE/AM0C00023_0006.JPEG.
16. He, W.; Li, G.; Zhang, S.; Wei, Y.; Wang, J.; Li, Q.; Zhang, X. Polypyrrole/Silver Coaxial Nanowire Aero-Sponges for Temperature-Independent Stress Sensing and Stress-Triggered Joule Heating. ACS Nano 2015, 9, 4244–4251, doi:10.1021/ACSNANO.5B00626/SUPPL_FILE/NN5B00626_SI_002.AVI.
17. Si, Y.; Wang, X.; Yan, C.; Yang, L.; Yu, J.; Ding, B. Ultralight Biomass-Derived Carbonaceous Nanofibrous Aerogels with Superelasticity and High Pressure-Sensitivity. Advanced Materials 2016, 28, 9512–9518, doi:10.1002/ADMA.201603143.
18. Tan, Y.; Liu, X.; Tang, W.; Chen, J.; Zhu, Z.; Li, L.; Zhou, N.; Kang, X.; Xu, D.; Wang, L.; et al. Flexible Pressure Sensors Based on Bionic Microstructures: From Plants to Animals. Adv Mater Interfaces 2022, 9, 2101312, doi:10.1002/ADMI.202101312.
19. Zhao, T.; Yuan, L.; Li, T.; Chen, L.; Li, X.; Zhang, J. Pollen-Shaped Hierarchical Structure for Pressure Sensors with High Sensitivity in an Ultrabroad Linear Response Range. ACS Appl Mater Interfaces 2020, 12, 55362–55371, doi:10.1021/ACSAMI.0C14314/ASSET/IMAGES/LARGE/AM0C14314_0006.JPEG.
20. Choong, C.; Shim, M.; Lee, B.; … S.J.-A.; 2014, undefined Highly Stretchable Resistive Pressure Sensors Using a Conductive Elastomeric Composite on a Micropyramid Array. Wiley Online Library 2014, 26, 3451–3458, doi:10.1002/adma.201305182.
21. Kim, S.W.; Lee, J.H.; Ko, H.J.; Lee, S.; Bae, G.Y.; Kim, D.; Lee, G.; Lee, S.G.; Cho, K. Mechanically Robust and Linearly Sensitive Soft Piezoresistive Pressure Sensor for a Wearable Human-Robot Interaction System. ACS Nano 2024, 18, 3151–3160, doi:10.1021/ACSNANO.3C09016/ASSET/IMAGES/LARGE/NN3C09016_0005.JPEG.
22. Peng, S.; Blanloeuil, P.; Wu, S.; Wang, C.H. Rational Design of Ultrasensitive Pressure Sensors by Tailoring Microscopic Features. Adv Mater Interfaces 2018, 5, 1800403, doi:10.1002/ADMI.201800403.
23. Gao, Y.; Lu, C.; Guohui, Y.; Sha, J.; Tan, J.; Xuan, F. Laser Micro-Structured Pressure Sensor with Modulated Sensitivity for Electronic Skins. Nanotechnology 2019, 30, 325502, doi:10.1088/1361-6528/AB1A86.
24. Wang, X.; Gu, Y.; Xiong, Z.; Cui, Z.; Zhang, T. Silk-Molded Flexible, Ultrasensitive, and Highly Stable Electronic Skin for Monitoring Human Physiological Signals. Advanced Materials 2014, 26, 1336–1342, doi:10.1002/ADMA.201304248.
25. Shi, J.; Wang, L.; Dai, Z.; Zhao, L.; Du, M.; Li, H.; Fang, Y. Multiscale Hierarchical Design of a Flexible Piezoresistive Pressure Sensor with High Sensitivity and Wide Linearity Range. Small 2018, 14, 1800819, doi:10.1002/SMLL.201800819.